Scientific Reports

https://doi.org/10.1038/s41598-025-33550-1

Article in Press

Investigation of continuous and discontinuous carbon fibers in Joule-heated cement composites

Received: 22 October 2025

Accepted: 19 December 2025

Published online: 22 December 2025

Cite this article as: Alsamori R. & Ozturk M. Investigation of continuous and discontinuous carbon fibers in Joule-heated cement composites. *Sci Rep* (2025). https://doi.org/10.1038/s41598-025-33550-1

Rawan Alsamori & Murat Ozturk

We are providing an unedited version of this manuscript to give early access to its findings. Before final publication, the manuscript will undergo further editing. Please note there may be errors present which affect the content, and all legal disclaimers apply.

If this paper is publishing under a Transparent Peer Review model then Peer Review reports will publish with the final article.

ARTICLE IN PRESS

© The Author(s) 2025. **Open Access** This article is licensed under a Creative Commons Attribution-NonCommercial-NoDerivatives 4.0 International License, which permits any non-commercial use, sharing, distribution and reproduction in any medium or format, as long as you give appropriate credit to the original author(s) and the source, provide a link to the Creative Commons licence, and indicate if you modified the licensed material. You do not have permission under this licence to share adapted material derived from this article or parts of it. The images or other third party material in this article are included in the article's Creative Commons licence, unless indicated otherwise in a credit line to the material. If material is not included in the article's Creative Commons licence and your intended use is not permitted by statutory regulation or exceeds the permitted use, you will need to obtain permission directly from the copyright holder. To view a copy of this licence, visit http://creativecommons.org/licenses/by-nc-nd/4.0/.

ARTICLE IN PRESS

Investigation of Continuous and Discontinuous Carbon Fibers in Joule-Heated Cement Composites

Rawan ALSAMORI[1] and Murat OZTURK[1]*

[1] Smart Materials Laboratory, Bursa Uludag University, Engineering Faculty, Civil Engineering, Bursa 16059, Türkiye

* Corresponding author. ORCID ID: 0000-0003-3389-4883; Email: muratozturk@uludag.edu.tr

Abstract

This study examines the Joule heating performance of carbon fiber-reinforced cement pastes to advance multifunctional building materials with self-heating and de-icing capabilities. Discontinuous (5, 10, and 15 mm) and continuous (150 mm) carbon fibers were compared under identical mixing and testing conditions. Specimens were prepared with fiber volume fractions of 0.21%, 0.28%, and 0.35%, and water-to-cement ratios of 0.30, 0.40, and 0.50. Alternating current voltages of 30, 45, and 60 V were applied for 45 minutes, and surface temperatures were monitored via infrared thermography. Discontinuous fibers demonstrated superior heating efficiency compared to continuous fibers. The maximum temperature of 64 °C was achieved with 0.35% 10 mm fibers at 0.30 w/c and 60 V, while continuous fiber specimens reached only 28 °C under the same conditions. Fiber length also influenced heating: at 0.40 w/c and 0.35% fiber content, 15 mm fibers reached 57.0 °C versus 49.4 °C (10 mm) and 41.1 °C (5 mm). Increasing w/c ratios consistently reduced performance. The results reveal that randomly oriented, discontinuous fibers yield significantly greater resistive heating than continuous fibers, particularly under higher voltage and lower porosity. These findings offer practical insights for optimizing fiber geometry and matrix design in conductive cement composites intended for thermal functionality.

Keywords: Cement paste; self-heating; carbon fiber; fiber length; Joule heating

1. Introduction

Cement-based composites have been extensively utilized in the construction industry and are regarded as fundamental materials due to their favorable balance of cost-effectiveness, widespread availability, mechanical strength, and long-term durability [1]. These materials are predominantly employed in load-bearing structural components such as bridges [2], dams [3], tunnels [4],

ARTICLE IN PRESS

pavements [5], and residential infrastructures, where their primary function is to sustain mechanical loads.

In recent years, increasing emphasis has been placed on developing construction materials that fulfill not only structural roles but also provide additional functional capabilities [6–9]. The evolving demands of modern infrastructure—driven by sustainability, energy efficiency, and resilience—have shifted material design paradigms toward multifunctionality. Materials that simultaneously serve mechanical, thermal, electrical, or self-responsive functions are classified as multifunctional materials, and their adoption is gaining traction in the built environment [10–12].

Multifunctional cement-based composites are engineered to offer auxiliary properties beyond their mechanical functions. These may include self-sensing (stress/strain, temperature etc.) [13–19], self-healing [20–22], thermal energy storage [23–26], electromagnetic shielding [27–30], and self-heating [31–33]. Among these, the self-heating capability is of particular interest, especially in climates where thermal management is critical. Self-heating cementitious materials can generate heat when an electrical potential is applied, allowing them to perform functions such as accelerated curing in low-temperature conditions, ice melting or anti-icing on road surfaces, and supplementary space heating in buildings [31].

The underlying mechanism enabling this thermal response is the Joule heating effect (also referred to as Ohmic or resistive heating), wherein electrical energy is converted into heat as charge carriers move through a conductive medium and undergo frequent collisions [34]. For this mechanism to be activated in cementitious matrices—which are inherently insulating in nature—the electrical conductivity of the composite must be significantly enhanced.

This enhancement is typically achieved by incorporating electrically conductive fillers into the cement matrix. Additives such as carbon fibers, steel fibers, graphite, and graphene have been widely investigated due to their high electrical conductivity and compatibility with cementitious environments [35–39]. However, it has also been reported in the literature that despite their excellent electrical conductivity, carbon fibers may exhibit poor compatibility with cement matrices, particularly due to limited interfacial bonding and dispersion issues [40,41]. Conductive fillers are introduced in either particulate or fibrous form and are intended to establish percolating conductive networks within the composite. However, achieving a homogeneous dispersion of these conductive phases remains a substantial challenge, particularly with discontinuous fibrous fillers, which tend to agglomerate or distribute unevenly [42–44].

ARTICLE IN PRESS

Although prior research has demonstrated the feasibility of imparting self-heating capabilities to carbon fiber-reinforced cement-based composites, a comprehensive understanding of how microstructural and compositional factors influence thermal behavior is still evolving. Parameters such as fiber volume fraction, fiber length, spatial distribution, and internal porosity are known to affect electrical conductivity and, consequently, heating efficiency. Recent work on UHPC reinforced with stainless steel wires has shown that microscale, high–aspect-ratio wires can establish an extensive electrically and thermally conductive network within the matrix [45], yet such systems do not address how fiber continuity versus discontinuity, variations in fiber length, or changes in matrix porosity govern electrothermal response.

Based on these gaps, the following measurable research hypotheses are proposed: (i) discontinuous fibers provide higher resistive heating efficiency per unit conductivity compared with continuous fibers; (ii) increasing fiber length reduces electrical resistivity and increases heating efficiency; (iii) increasing fiber dosage enhances heating performance up to the percolation range; and (iv) higher matrix porosity decreases heating efficiency by increasing electrical resistance.

To address these hypotheses, the present study investigates the self-heating performance of cement-based composites containing both discontinuous (short) and continuous (long) carbon fibers. While short fibers are uniformly mixed throughout the matrix to facilitate isotropic conduction, continuous fibers are embedded in bundled configurations to explore anisotropic conduction behavior. The thermal responses of the prepared composites are systematically evaluated under applied voltages of 30 V, 45 V, and 60 V over a 45-minute heating cycle. The objective is to correlate the fiber characteristics and composite microstructure with the efficiency and stability of resistive heating, thereby contributing to the design of next-generation multifunctional construction materials.

2. Materials and methods

In this experimental program, cementitious composites are produced using Ordinary Portland Cement (CEM I 42.5 R), potable tap water, and electrically conductive carbon fibers. All materials are locally sourced: cement is supplied by Bursa Çimento (Bursa, Turkey), and 24 K carbon fibers are provided by DowAksa (Yalova, Turkey). The carbon fibers have a nominal diameter of 7 μm, a tensile strength exceeding 4900 MPa, and an electrical resistivity of approximately 1.6×10^{-3} Ω·cm.

ARTICLE IN PRESS

Both chopped (5 mm, 10 mm, and 15 mm) and continuous (150 mm) carbon fibers are incorporated into the mixtures. Fiber volume fractions are adjusted to 0.21%, 0.28%, and 0.35% in order to investigate the influence of fiber dosage. For mixtures with continuous fibers, 3, 4, and 5 fiber bundles are used depending on the target fiber volume fraction, with equal spacing maintained between bundles in all configurations. Each continuous fiber bundle corresponds to an uncut commercial carbon fiber tow composed of filaments with an average diameter of approximately 7 μm and a length of about 150 mm, and the target fiber volume fractions were achieved by adjusting the number of such bundles. The comparison between continuous fiber bundles and dispersed chopped fibers does not assume that both systems create the same electrical conditions. The aim is simply to use the same total amount of carbon fiber in each configuration. By keeping the fiber volume fraction equal, the study isolates how the two different network structures influence heating performance. Continuous bundles guide the current along a narrow path, while chopped fibers spread the resistance throughout the matrix. This difference is intentional, because the objective is to show how network morphology—not fiber quantity—affects Joule heating. These specific fiber dosages are selected to explore a range below and above expected percolation thresholds while ensuring uniform fiber dispersion. Preliminary trials indicated that beyond 0.35%, fiber agglomeration hindered homogeneous mixing. Additionally, the continuous fiber bundles are placed using a fixed alignment guide that ensured parallel orientation along the mold axis, with controlled center-to-center spacing and unaltered bundle packing, allowing the reported fiber contents to correspond to precise and reproducible geometric configurations. Matrix compositions are designed with water-to-cement (w/c) ratios of 0.30, 0.40, and 0.50 to represent different levels of workability and porosity. The detailed mix proportions are given in Table 1. Continuous fibers are not included in the fiber length analysis because they represent a different conductive network architecture rather than an extension of chopped fiber length. The length study is therefore restricted to discontinuous fibers to isolate length effects within a single network type.

Table 1. Mix design details (Mix IDs reflect water-to-cement ratio, fiber length, and fiber quantity. For example, ‘0.3-10mm4DSZ’ indicates w/c ratio = 0.30, 10 mm fiber length, and 4 fiber bundles (or equivalent chopped fiber content). ‘DSZ’ refers to discontinuous fibers, while ‘DSL’ denotes continuous fiber bundles.)

ARTICLE IN PRESS

Mix ID	w/c Ratio	Fiber Length (mm)	Fiber Volume Fraction (%)	Fiber Form	Continuous/ Discontinuous
0.3-10mm3DSZ	0.30	10	0.21	Chopped Fiber	Discontinuous
0.3-10mm4DSZ	0.30	10	0.28	Chopped Fiber	Discontinuous
0.3-10mm5DSZ	0.30	10	0.35	Chopped Fiber	Discontinuous
0.4-10mm3DSZ	0.40	10	0.21	Chopped Fiber	Discontinuous
0.4-10mm4DSZ	0.40	10	0. 28	Chopped Fiber	Discontinuous
0.4-10mm5DSZ	0.40	10	0.35	Chopped Fiber	Discontinuous
0.5-10mm3DSZ	0.50	10	0.21	Chopped Fiber	Discontinuous
0.5-10mm4DSZ	0.50	10	0. 28	Chopped Fiber	Discontinuous
0.5-10mm5DSZ	0.50	10	0.35	Chopped Fiber	Discontinuous
0.3 3DSL	0.30	150	0.21	3 Fiber Bundle	Continuous
0.3 4DSL	0.30	150	0. 28	4 Fiber Bundle	Continuous
0.3 5DSL	0.30	150	0.35	5 Fiber Bundle	Continuous
0.4 3DSL	0.40	150	0.21	3 Fiber Bundle	Continuous
0.4 4DSL	0.40	150	0. 28	4 Fiber Bundle	Continuous
0.4 5DSL	0.40	150	0.35	5 Fiber Bundle	Continuous
0.5 3DSL	0.50	150	0.21	3 Fiber Bundle	Continuous
0.5 4DSL	0.50	150	0. 28	4 Fiber Bundle	Continuous
0.5 5DSL	0.50	150	0.35	5 Fiber Bundle	Continuous
0.4-5mm4DSZ	0.40	5	0. 28	Chopped Fiber	Discontinuous
0.4-5mm4DSZ	0.40	15	0. 28	Chopped Fiber	Discontinuous

ARTICLE IN PRESS

Mixing is performed using a laboratory-scale Hobart mixer. Initially, dry components—cement and carbon fibers—are blended at a low speed (100 rpm) for 1 minute to ensure preliminary dispersion. Subsequently, water is gradually added, and mixing is continued at a higher speed (300 rpm) for four additional minutes until a uniform and homogeneous paste is obtained. To maintain consistent dispersion across all specimens, the same mixing procedure is applied to every batch.

ARTICLE IN PRESS

Uniformity is visually verified during mixing, with no observable fiber clumping or sedimentation prior to casting.

The fresh mixtures are poured into oiled wooden molds with internal dimensions of 150 mm × 150 mm × 50 mm. A two-step casting procedure is applied to ensure the proper placement of copper mesh electrodes. First, the mold is half-filled with the fresh mix and subjected to vibration to eliminate entrapped air. After the composite begins to set, the electrodes are carefully placed, and the remaining mixture is cast. This method ensures precise and stable electrode positioning.

Copper mesh electrodes with a thickness of 0.2 mm and a mesh size of 30 mesh are embedded in the specimens. Electrode strips are sized as 0.2 mm × 15 mm × 180 mm. The configuration of the electrodes is determined based on the fiber form:

For composites with continuous fibers, fiber bundles are first attached to the copper mesh electrodes using silver paint to ensure effective electrical contact. The electrodes are placed perpendicular to the specimen thickness and aligned in a coplanar configuration, allowing current to flow along the plane of the fiber layout. The term coplanar electrode configuration refers to two copper mesh electrodes embedded on the same surface of the prism specimen, positioned parallel to each other with a fixed center-to-center spacing. Both electrodes lie in the same geometric plane, producing a two-dimensional current flow during resistivity and heating tests. Different electrode configurations are used because the current paths required to activate continuous and discontinuous fiber networks are inherently different. The selected configurations ensure effective current flow for each fiber architecture rather than enforcing identical electrode geometry. A photograph of the electrodes with four bundles of continuous carbon fibers is presented in Figure 1.

ARTICLE IN PRESS

ARTICLE IN PRESS

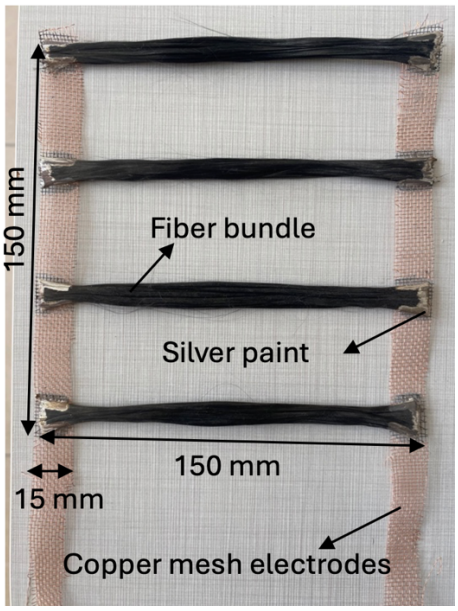

Figure 1. Photographic view of the electrodes with four bundles of continuous carbon fibers.

For composites containing chopped (discontinuous) fibers, no silver paint is applied. The two copper mesh electrodes are placed parallel to the specimen thickness and embedded in a sandwich configuration, allowing current to flow across the height of the sample.

For discontinuous-fiber specimens, the objective was to ensure good contact between the composite surface and the electrodes. The mesh structure of the copper electrodes provide sufficient interlocking at the electrode interface; therefore, no silver paint was required. In contrast, for continuous-fiber specimens, the main requirement is to ensure a high-quality electrical connection between the fiber bundle and the electrode face. For this reason, a thin layer of silver paint is applied on the electrode surface prior to casting. The silver paint is not expected to increase the interface resistance. This approach keeps the electrode–specimen contact conditions consistent across all mixes, preventing variations in contact resistance from influencing the heating results.

After 24 hours of setting, the specimens are demolded and immersed in a water-filled curing tank at ambient temperature. The curing process is continued for 28 days to ensure adequate hydration and strength development.

Before thermal testing, all specimens are dried in a ventilated oven at 50 °C to minimize internal moisture content, which may otherwise interfere with electrical conductivity or temperature readings. A moderate drying temperature is chosen to avoid potential microstructural degradation.

ARTICLE IN PRESS

Residual moisture content is not quantified, as drying is applied uniformly to ensure comparable testing conditions rather than to evaluate moisture-dependent conductivity effects.

Heating tests are carried out using an alternating current (AC) power supply (GW Instek ASR-2050). Voltage levels are set at 30 V, 45 V, and 60 V, and the AC frequency is kept constant at 50 Hz for all specimens. Any capacitive or impedance-related effects remain consistent across all specimens and therefore do not influence the relative comparison of heating behavior. Each test is conducted for 45 minutes, with temperature measurements recorded at 15-minute intervals, and this fixed duration is used to ensure identical exposure conditions for all specimens, acknowledging that it does not necessarily correspond to thermal stabilization for every mix but provides a consistent basis for comparative evaluation. Electrical resistivity measurements are not included in this study because the objective is to compare the heating behavior of different fiber network architectures under identical electrical input conditions. In cementitious composites, heating performance is affected not only by bulk conductivity but also by fiber arrangement and contact resistance. Thermal cycling or repeatability tests were not performed, and the results therefore represent only the first-cycle heating response; conducting such tests would be beneficial for assessing potential changes in resistive or microstructural stability under repeated operation. While capacitive effects and dielectric losses may occur under AC excitation, analyzing these impedance-related mechanisms falls outside the scope of the present work, and all specimens are tested under identical AC conditions so that any such effects remain the same across mixes. Surface temperature evolution is monitored using a high-resolution infrared thermal camera (Fluke TiS75+), which operates in the range of −20 °C to 550 °C with a thermal resolution of 384 × 288 pixels. Data are acquired using FLUKE Connect software, and average surface temperatures are computed across the entire exposed specimen area. All infrared measurements are conducted using a fixed camera-to-specimen distance of 0.50 m and an emissivity setting of 0.95. The camera is aligned perpendicular to the specimen surface, and these parameters are kept constant for all tests to ensure repeatability and consistency in temperature measurements. Infrared measurements are performed using a fixed camera distance, emissivity setting, and alignment for all specimens. Since the study focuses on comparative surface temperature response rather than detailed spatial gradient analysis, relative temperature differences are considered reliable under these consistent measurement conditions. Surface temperature is monitored using infrared thermography to enable consistent comparison of heating behavior under identical boundary conditions. Although internal temperature measurements could capture through-thickness gradients, surface-averaged infrared

ARTICLE IN PRESS

measurements are considered adequate for relative evaluation, as emissivity settings, convection conditions, and camera parameters are kept constant for all specimens. Thermal conductivity is not measured in this study because evaluating heat-dissipation behavior falls outside the scope. The work focuses on how fiber type, fiber length, and matrix composition influence heating under identical boundary conditions. Although conductivity data could provide helpful supplementary insight, the comparative conclusions remain valid since all specimens experience the same heat-loss environment.

Instead of using a single-point measurement, the reported temperature corresponds to the average of the entire exposed surface, which is considered adequate for representing the heating performance under the controlled test conditions. Although internal temperature can also be measured to capture through-thickness gradients, this study intentionally adopts surface-based averaging as the selected measurement approach. The interpretation of anisotropic conduction in continuous-fiber specimens is based on the geometric alignment of the long, uncut bundles, which create a preferential in-plane pathway between electrodes. Although this layout implies directional conductivity, independent in-plane and through-thickness resistivity measurements are not performed. The resulting discussion is therefore qualitative, and a complete verification of anisotropy requires direction-dependent electrical testing to be examined in subsequent studies.

Figure 2 presents a representative specimen with embedded electrodes, while a schematic representation of the test setup is provided in Figure 3. A minimum of three specimens were tested for each mix to ensure the reliability of the results.

ARTICLE IN PRESS

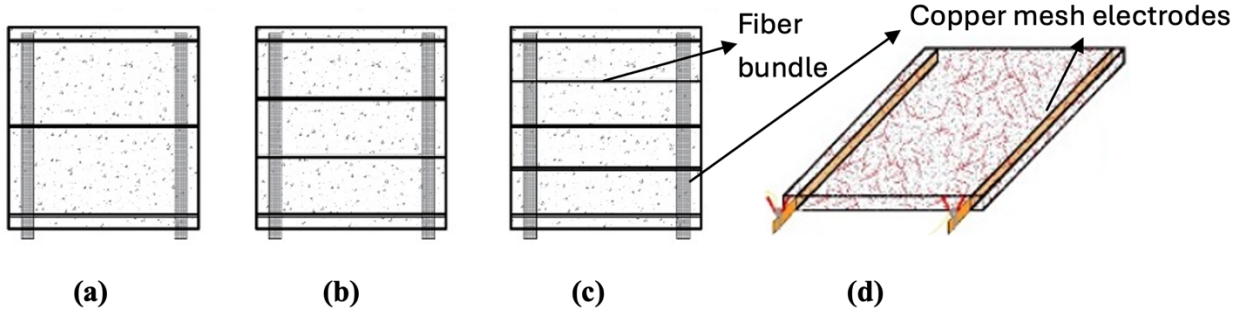

Figure 2. Cement paste specimens containing: a) 3 bundles of carbon fibers, b) 4 bundles of carbon fibers, c) 5 bundles of carbon fibers, and d) chopped (discontinuous) carbon fibers.

ARTICLE IN PRESS

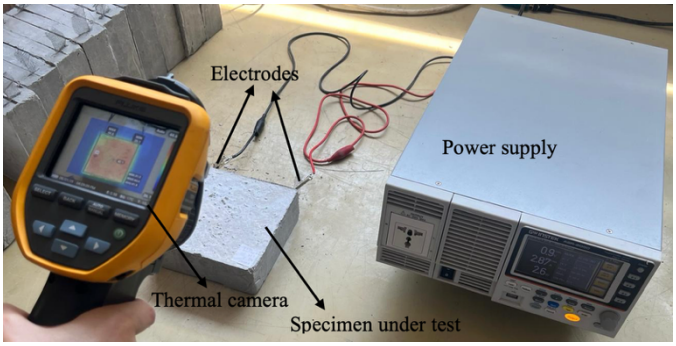

Figure 3. Self-heating measurement setup

3. Results and discussion

The study investigates the thermal behavior of cement paste composites incorporating carbon fibers under different applied voltages—30 V, 45 V, and 60 V. To understand the effects of fiber type, volume fraction, and matrix porosity, three carbon fiber dosages (0.21%, 0.28%, and 0.35% by volume) were combined with two distinct fiber configurations: continuous fibers bundled to match volume fractions and randomly dispersed short fibers. All specimens were tested at water-to-cement (w/c) ratios of 0.30, 0.40, and 0.50, and their surface temperatures were monitored over 15, 30, and 45 minutes. Sample identifiers in the dataset follow a consistent labeling structure. The initial value denotes the w/c ratio, followed by the number of fiber bundles (or their volumetric equivalents for discontinuous fibers), then the fiber type (DSZ for discontinuous, DSL for continuous), followed by the heating duration (in minutes), and finally the applied voltage. For example, the label "0.3 3DSZ 15 min 30V" refers to a sample with a 0.30 w/c ratio, containing 0.21% volume of discontinuous fibers (equivalent to 3 bundles), heated for 15 minutes under 30 V. The control specimens, defined as fiber-free cement paste samples, remained at 22 °C throughout the tests and appear in the plots as a flat baseline line, showing no heating response under any of the applied voltages or exposure durations.

Figure 4 provides representative thermograms recorded during the heating tests, illustrating the surface temperature distribution for a specimen reinforced with short fibers (a) and a specimen containing three continuous fiber bundles (b). Although strict thermal equilibrium is not explicitly verified, the temperature–time curves exhibites a marked reduction in heating rate near the 45-minute mark, indicating an approach to quasi-steady thermal behavior suitable for comparative evaluation. The short-fiber specimen exhibits a more uniform and evenly distributed temperature

ARTICLE IN PRESS

field, whereas the bundled-fiber specimen shows localized heating aligned with the bundle direction, reflecting the anisotropic conduction paths formed by the continuous fibers.

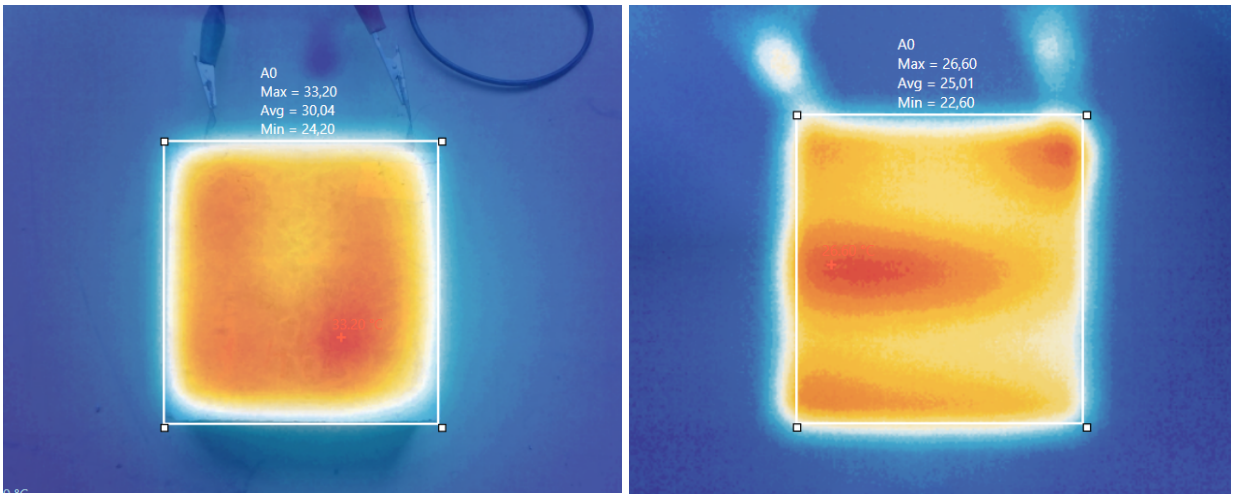

(a) (b)

Figure 4. The thermograms taken by the thermometer a) specimen with short fiber, b) specimen with 3 bundles of carbon fiber

Under an applied potential of 30 V, shown in Figure 4, notable differences were observed between specimens reinforced with continuous and discontinuous fibers. At the lowest fiber dosage of 0.21% (Figure 4(a)), composites containing short fibers displayed significantly better heating performance. For specimens with a w/c ratio of 0.30, surface temperatures reached approximately 32 °C after 45 minutes, while those reinforced with continuous fibers remained around 28 °C. Similar patterns were noted at w/c ratios of 0.40 and 0.50, albeit with lower final temperatures. This implies that at lower fiber volumes, randomly oriented fibers generate greater internal resistance, promoting localized Joule heating [46]. This is because limited fiber connectivity at low dosages forces current through higher-resistance paths, increasing localized heating.

When the fiber volume was increased to 0.28% (Figure 4(b)), discontinuous fiber composites again exhibited superior thermal performance. Temperatures reached around 33 °C at a 0.30 w/c ratio, compared to 29 °C in continuous fiber specimens. Although higher fiber content generally improves the formation of conductive pathways, continuous fibers tend to form direct current routes with minimal resistance, thereby reducing the potential for heat generation. In contrast, short fibers, due to their irregular distribution and contact resistance, create more resistive paths that boost thermal output. As with lower fiber content, increasing the w/c ratio continued to reduce

ARTICLE IN PRESS

temperature gains across both fiber types, primarily due to increased porosity and disrupted conductivity [47].

The highest fiber dosage, 0.35%, produced the most significant thermal contrast (Figure 4(c)). Specimens reinforced with discontinuous fibers reached approximately 42 °C at a 0.30 w/c ratio, while continuous fiber composites plateaued at 30 °C. This trend held across all w/c ratios, although increasing water content led to a consistent drop in surface temperature. For example, in short-fiber specimens at a 0.50 w/c ratio, temperatures fell to around 33–34 °C, indicating the substantial role of matrix porosity and water content in modulating electrical and thermal response. This temperature reduction can be attributed to increased matrix porosity at higher w/c ratios, which disrupts conductive fiber networks and introduces more non-conductive zones. As porosity rises, electrical continuity decreases, resulting in lower current flow and thus reduced Joule heating efficiency. Current and power measurements were not recorded during the heating tests because the focus of this study is a comparative evaluation of thermal response under identical applied voltage and boundary conditions, rather than a calculation of absolute power dissipation. Accordingly, heating performance is discussed in a relative sense based on temperature evolution, not in terms of power-based efficiency.

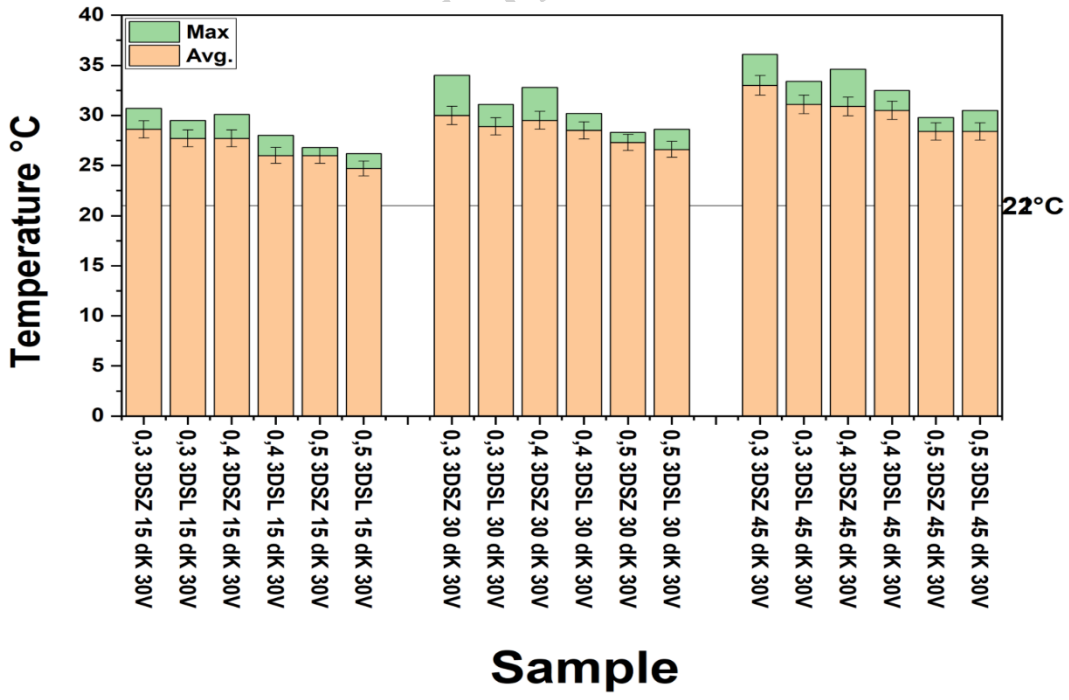

(a)

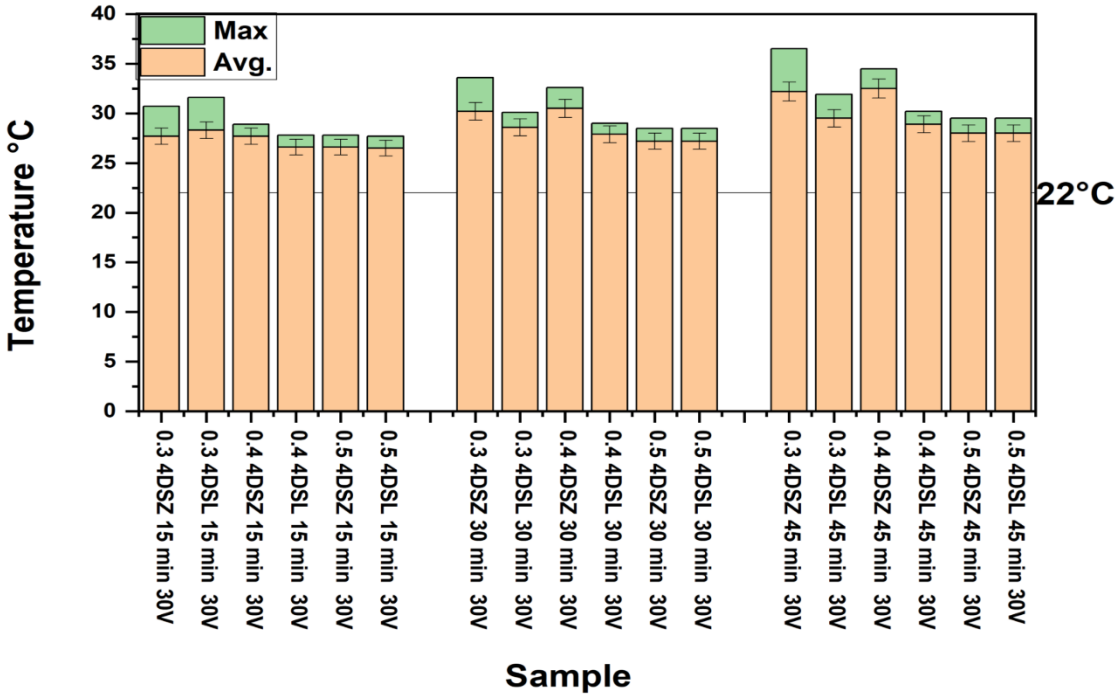
Max
Avg.
Temperature °C
22°C
Sample
0.3 4DSZ 15 min 30V
0.3 4DSL 15 min 30V
0.4 4DSZ 15 min 30V
0.4 4DSL 15 min 30V
0.5 4DSZ 15 min 30V
0.5 4DSL 15 min 30V
0.3 4DSZ 30 min 30V
0.3 4DSL 30 min 30V
0.4 4DSZ 30 min 30V
0.4 4DSL 30 min 30V
0.5 4DSZ 30 min 30V
0.5 4DSL 30 min 30V
0.3 4DSZ 45 min 30V
0.3 4DSL 45 min 30V
0.4 4DSZ 45 min 30V
0.4 4DSL 45 min 30V
0.5 4DSZ 45 min 30V
0.5 4DSL 45 min 30V

(b)

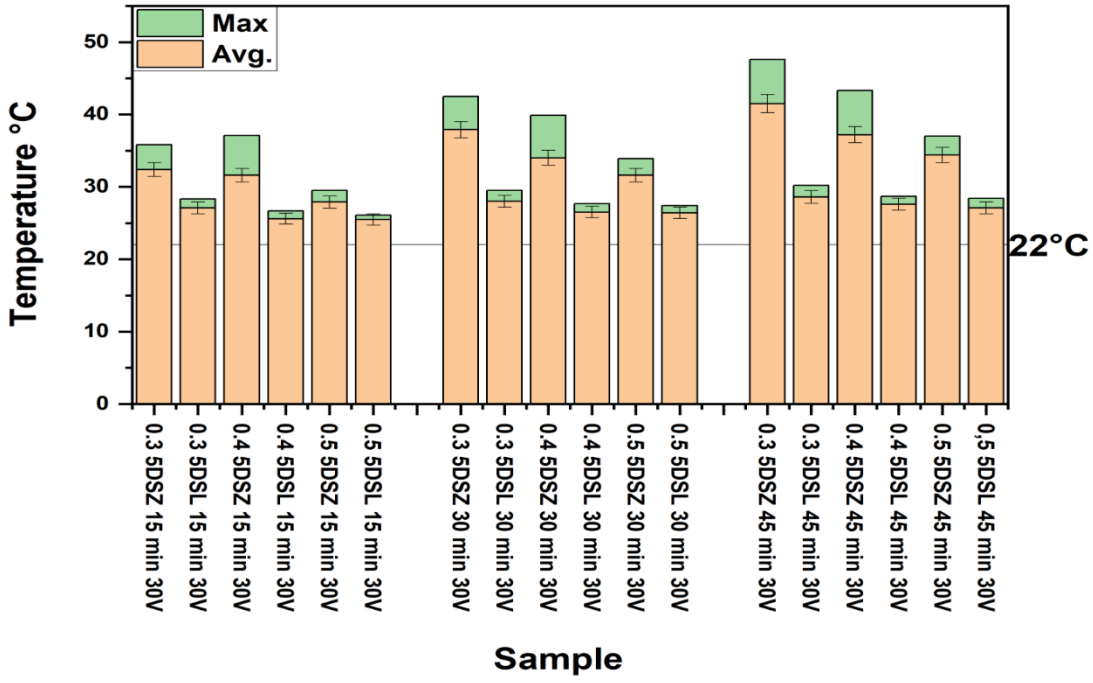
Max
Avg.
Temperature °C
22°C
Sample
0.3 5DSZ 15 min 30V
0.3 5DSL 15 min 30V
0.4 5DSZ 15 min 30V
0.4 5DSL 15 min 30V
0.5 5DSZ 15 min 30V
0.5 5DSL 15 min 30V
0.3 5DSZ 30 min 30V
0.3 5DSL 30 min 30V
0.4 5DSZ 30 min 30V
0.4 5DSL 30 min 30V
0.5 5DSZ 30 min 30V
0.5 5DSL 30 min 30V
0.3 5DSZ 45 min 30V
0.3 5DSL 45 min 30V
0.4 5DSZ 45 min 30V
0.4 5DSL 45 min 30V
0.5 5DSZ 45 min 30V
0,5 5DSL 45 min 30V

(c)

ARTICLE IN PRESS

Figure 4. Heating performance of cement paste specimens containing continuous and discontinuous carbon fibers and prepared with different water-to-cement ratios (0.30, 0.40, and 0.50) under an applied voltage of 30 V: a) specimens with 0.21% carbon fiber by volume, b) specimens with 0.28% carbon fiber by volume, c) specimens with 0.35% carbon fiber by volume.

To explore the influence of electrical intensity, the same test configurations were repeated under a higher voltage of 45 V (Figure 5). Across all fiber volumes and w/c ratios, an overall increase in surface temperature was observed compared to the 30 V case. At 0.21% fiber content (Figure 5(a)), discontinuous fiber composites achieved average temperatures between 38–40 °C, with maximum values nearing 45 °C. Continuous fiber specimens also showed improvements but remained consistently below 36 °C. This suggests that while increased voltage enhances thermal output across the board, fiber morphology remains a dominant factor in determining heating performance.

The 0.28% fiber group showed a greater response to the elevated input (Figure 5(b)). Discontinuous fiber composites reached peak temperatures close to 42 °C at a 0.30 w/c ratio, with average values consistently higher than those of continuous fiber mixes, which hovered around 25–28 °C. These results further validate the premise that resistive heating is more effective in matrices where electrical flow is interrupted and redirected through fiber contacts, a scenario more common in randomly dispersed fiber systems [48,49]. In such systems, the absence of continuous conductive paths forces electrons to travel through multiple fiber–fiber interfaces, each introducing contact resistance. These repeated interruptions increase localized energy dissipation, thereby enhancing overall heat generation via the Joule effect. It should be noted that electrical conduction in fiber-reinforced cementitious composites may arise from a combination of contact resistance, tunneling conduction, and capacitive bridging; therefore, the observed heating behavior is discussed in a comparative rather than mechanistic-exclusive framework.

At the highest fiber content of 0.35% (Figure 5(c)), discontinuous fiber specimens demonstrated the most substantial increase in thermal performance. Surface temperatures exceeded 50 °C on average, with peaks reaching 55–59 °C in lower w/c mixes. Continuous fiber specimens, despite the increased voltage, again trailed behind with temperatures in the 25–28 °C range. These results suggest that fiber content and distribution have a synergistic effect under electrical stimulation: higher volumes of randomly oriented fibers form more numerous junctions and resistive nodes, thereby amplifying heat generation.

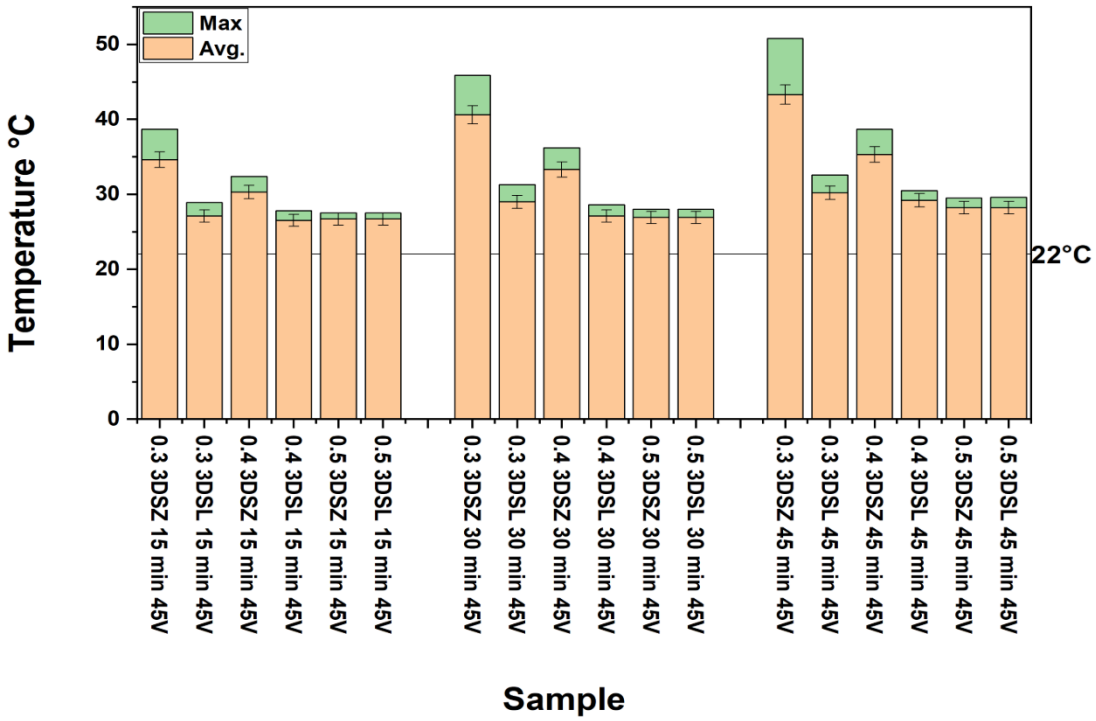
Max
Avg.
Temperature °C
0
10
20
30
40
50
22°C
0.3 3DSZ 15 min 45V
0.3 3DSL 15 min 45V
0.4 3DSZ 15 min 45V
0.4 3DSL 15 min 45V
0.5 3DSZ 15 min 45V
0.5 3DSL 15 min 45V
0.3 3DSZ 30 min 45V
0.3 3DSL 30 min 45V
0.4 3DSZ 30 min 45V
0.4 3DSL 30 min 45V
0.5 3DSZ 30 min 45V
0.5 3DSL 30 min 45V
0.3 3DSZ 45 min 45V
0.3 3DSL 45 min 45V
0.4 3DSZ 45 min 45V
0.4 3DSL 45 min 45V
0.5 3DSZ 45 min 45V
0.5 3DSL 45 min 45V
Sample

(a)

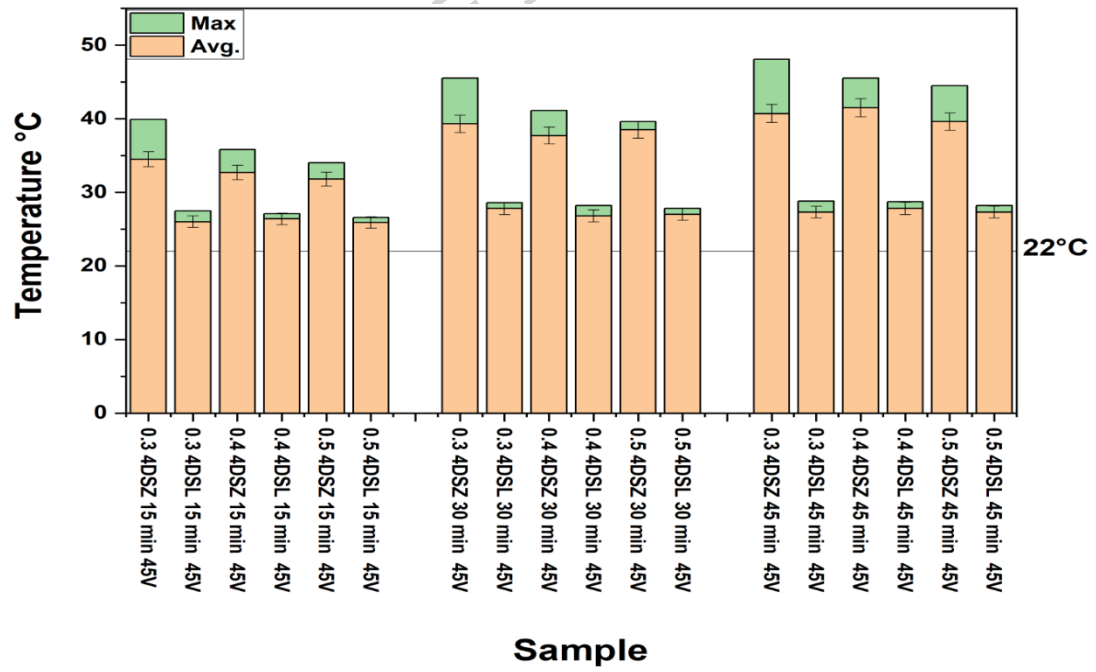
Max
Avg.
Temperature °C
0
10
20
30
40
50
22°C
0.3 4DSZ 15 min 45V
0.3 4DSL 15 min 45V
0.4 4DSZ 15 min 45V
0.4 4DSL 15 min 45V
0.5 4DSZ 15 min 45V
0.5 4DSL 15 min 45V
0.3 4DSZ 30 min 45V
0.3 4DSL 30 min 45V
0.4 4DSZ 30 min 45V
0.4 4DSL 30 min 45V
0.5 4DSZ 30 min 45V
0.5 4DSL 30 min 45V
0.3 4DSZ 45 min 45V
0.3 4DSL 45 min 45V
0.4 4DSZ 45 min 45V
0.4 4DSL 45 min 45V
0.5 4DSZ 45 min 45V
0.5 4DSL 45 min 45V
Sample

(b)

ARTICLE IN PRESS

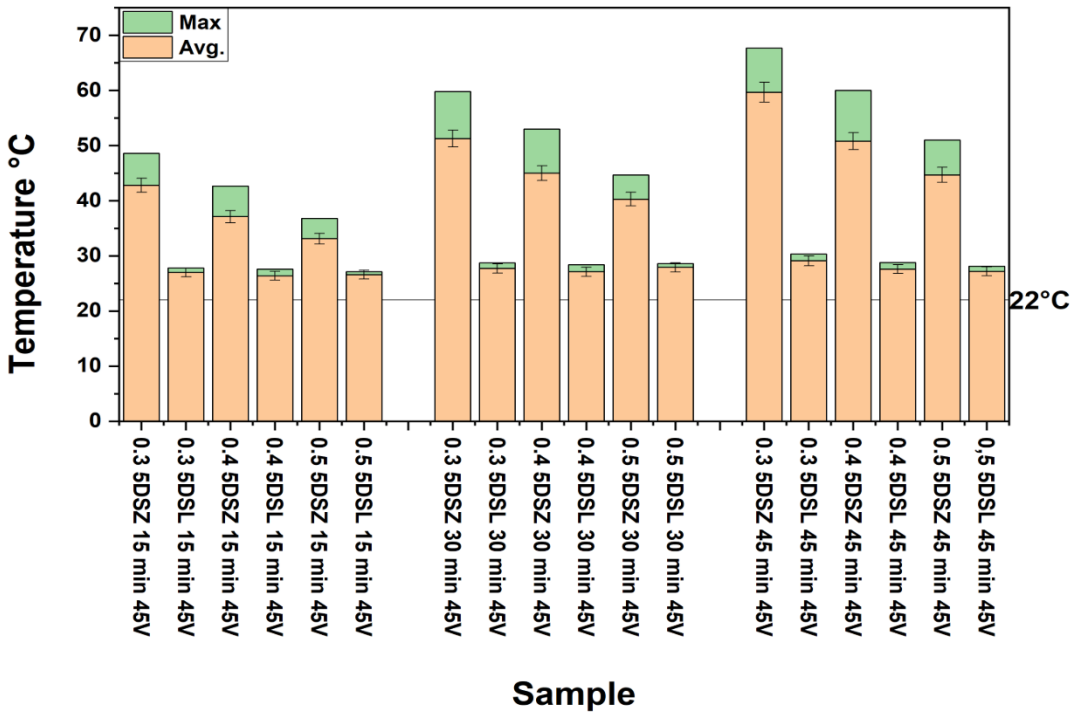

(c)

Figure 5. Heating performance of cement paste specimens containing continuous and discontinuous carbon fibers and prepared with different water-to-cement ratios (0.30, 0.40, and 0.50) under an applied voltage o45 V: a) specimens with 0.21% carbon fiber by volume, b) specimens with 0.28% carbon fiber by volume, c) specimens with 0.35% carbon fiber by volume.

A third set of experiments conducted under 60 V provided a deeper look at the upper bounds of thermal response (Figure 6). At 0.21% fiber content (Figure 6(a)), composites with short fibers reached surface temperatures of approximately 55 °C at a 0.30 w/c ratio, while continuous fiber mixes again stabilized near 29 °C. As the w/c ratio increased, the heating performance of short-fiber composites decreased to around 49 °C (w/c = 0.40) and 43 °C (w/c = 0.50), reinforcing the critical role of matrix porosity.

The 0.28% series (Figure 6(b)) showed an even stronger thermal response. Short-fiber composites with a 0.30 w/c ratio reached over 51 °C, while continuous fiber specimens remained near 28 °C, regardless of matrix composition. A similar pattern was evident at 0.40 and 0.50 w/c, where thermal gains in continuous fiber mixes were limited, highlighting their lower resistive characteristics and more stable but weaker heating capacity.

ARTICLE IN PRESS

At 0.35% fiber volume, discontinuous fiber composites delivered the highest recorded temperatures in the study (Figure 6(c)). With a 0.30 w/c ratio, these specimens exceeded 64 °C on average, while mixes containing continuous fibers stayed just below 28 °C. Even at elevated water contents (w/c = 0.40 and 0.50), short-fiber composites maintained high thermal output—around 54 °C and 52 °C, respectively—demonstrating the effectiveness of resistive heating through distributed current pathways. The maximum observed temperatures remains well below known degradation thresholds for hydrated cement paste, but the structural or long-term implications of localized heating are not evaluated here and would require dedicated mechanical and durability assessment. Continuous fiber systems again showed minimal change with varying w/c ratios, suggesting that their thermal performance is less sensitive to matrix conductivity.

Taken as a whole, Figures 4 through 6 reveal several key insights. First, the heating efficiency of cement paste composites increases substantially with electrical input, but this benefit is most effectively harnessed when using discontinuous fibers. Their random distribution and contact resistance promote resistive heating, especially under higher voltages. Second, continuous fibers—despite providing direct conduction routes—limit thermal gain. This behavior can be attributed to anisotropic conduction. Continuous fibers form an aligned, low-resistance pathway that concentrates current along the fiber axis. This reduces transverse current flow into the surrounding matrix, limiting the distributed Joule heating generated through fiber–matrix and fiber–fibre interfaces. As a result, a considerable portion of the electrical energy is transported along the fiber direction rather than being dissipated as heat within the composite volume. Third, the water-to-cement ratio plays a consistently negative role in heating performance: higher w/c values increase matrix porosity, interrupt conductive networks, and limit the effectiveness of fiber connectivity. Lastly, increasing the volume fraction of carbon fibers enhances heating potential across all scenarios, though the gain is significantly more pronounced in discontinuous systems. This is because higher w/c ratios lead to increased porosity, which interrupts conductive fiber paths and reduces overall current flow. In addition, although increasing fiber content improves heating in both systems, the effect is stronger in discontinuous fibers due to more frequent fiber–fiber contacts that enhance resistive heating.

It is important to note that this study does not include impedance spectroscopy or current–voltage characterization. The experimental program focuses on comparing the thermal response of the composites under controlled electrical input rather than classifying the underlying conduction mechanism. While impedance or current-voltage data provide a direct way to distinguish

percolative, contact-controlled, or tunneling-based conduction, the heating trends observed here still offer clear evidence of how fiber morphology, fiber length, and matrix porosity influence the formation and efficiency of the conductive network. The consistent temperature evolution across all specimens indicates that the comparative conclusions remain valid even in the absence of electrical impedance measurements.

These findings emphasize that both fiber morphology and mix design must be carefully optimized when engineering electrically conductive cementitious composites intended for thermal applications. Achieving high-performance heating behavior requires not only sufficient fiber content but also a matrix that supports resistive pathways and maintains electrical continuity, particularly under high-voltage operation.

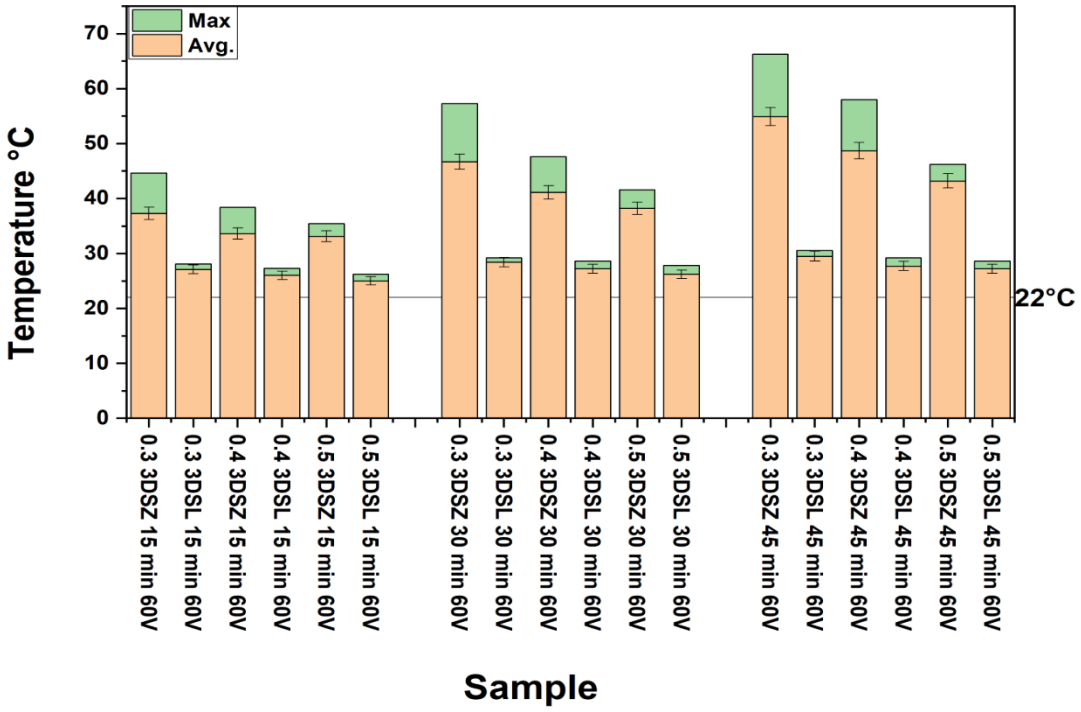

(a)

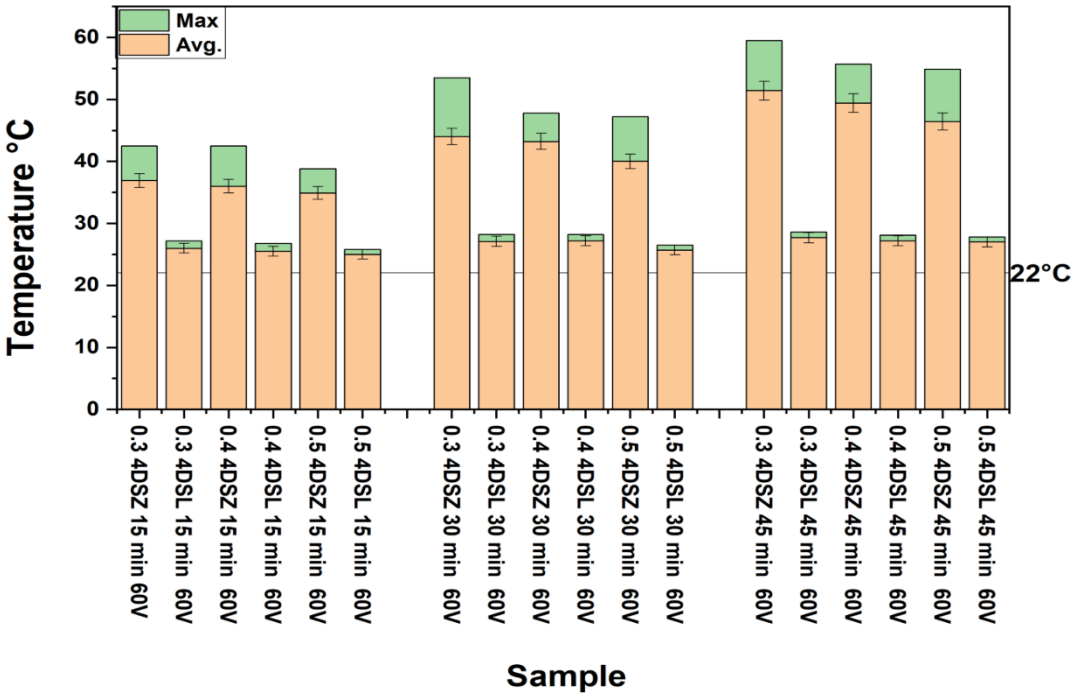
Max
Avg.
Temperature °C
0
10
20
30
40
50
60
22°C
0.3 4DSZ 15 min 60V
0.3 4DSL 15 min 60V
0.4 4DSZ 15 min 60V
0.4 4DSL 15 min 60V
0.5 4DSZ 15 min 60V
0.5 4DSL 15 min 60V
0.3 4DSZ 30 min 60V
0.3 4DSL 30 min 60V
0.4 4DSZ 30 min 60V
0.4 4DSL 30 min 60V
0.5 4DSZ 30 min 60V
0.5 4DSL 30 min 60V
0.3 4DSZ 45 min 60V
0.3 4DSL 45 min 60V
0.4 4DSZ 45 min 60V
0.4 4DSL 45 min 60V
0.5 4DSZ 45 min 60V
0.5 4DSL 45 min 60V
Sample

(b)

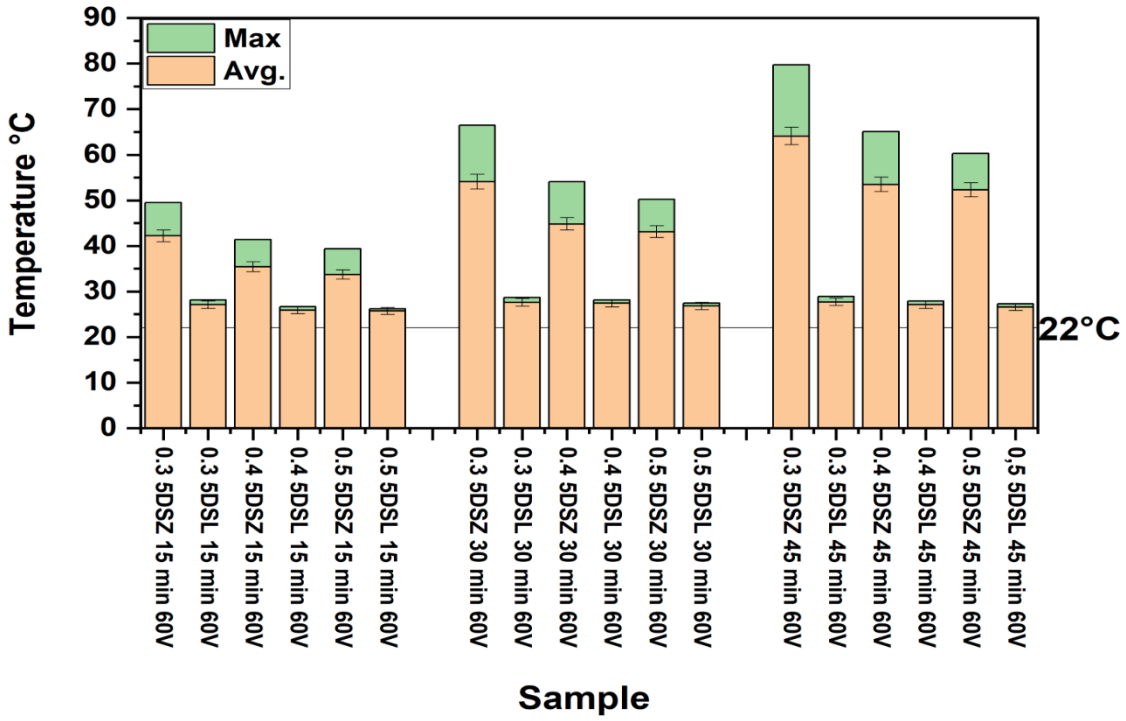
Max
Avg.
Temperature °C
0
10
20
30
40
50
60
70
80
90
22°C
0.3 5DSZ 15 min 60V
0.3 5DSL 15 min 60V
0.4 5DSZ 15 min 60V
0.4 5DSL 15 min 60V
0.5 5DSZ 15 min 60V
0.5 5DSL 15 min 60V
0.3 5DSZ 30 min 60V
0.3 5DSL 30 min 60V
0.4 5DSZ 30 min 60V
0.4 5DSL 30 min 60V
0.5 5DSZ 30 min 60V
0.5 5DSL 30 min 60V
0.3 5DSZ 45 min 60V
0.3 5DSL 45 min 60V
0.4 5DSZ 45 min 60V
0.4 5DSL 45 min 60V
0.5 5DSZ 45 min 60V
0,5 5DSL 45 min 60V
Sample

(c)

ARTICLE IN PRESS

Figure 6. Heating performance of cement paste specimens containing continuous and discontinuous carbon fibers and prepared with different water-to-cement ratios (0.30, 0.40, and 0.50) under an applied voltage of 60 V: a) specimens with 0.21% carbon fiber by volume, b) specimens with 0.28% carbon fiber by volume, c) specimens with 0.35% carbon fiber by volume.

To isolate the influence of carbon fiber length on the thermal behavior of cement-based composites, specimens with a fixed fiber volume fraction of 0.28% and a constant water-to-cement ratio of 0.40 were tested under applied voltages of 30 V, 45 V, and 60 V (Figure 7). Three fiber lengths—5 mm, 10 mm, and 15 mm—were considered. The average surface temperatures were recorded after 15, 30, and 45 minutes of exposure. The results clearly demonstrate that fiber length plays a critical role in thermal efficiency, especially under increasing electrical input.

At 30 V (Figure 7 (a)), the heating performance scaled directly with fiber length. After 45 minutes, specimens with 15 mm fibers reached an average temperature of 41.2 °C, compared to 32.5 °C for 10 mm fibers and only 29.7 °C for 5 mm. This trend was also observed at earlier time points, with the 15 mm fiber specimens consistently outperforming the others. The longer fibers appear to form more effective bridging (the term ‘bridging’ is used here as a qualitative interpretation based on macroscopic thermal response; direct microstructural verification of fiber interconnectivity was not performed and is identified as a limitation of the present study.)between conductive paths, enhancing resistive heating by increasing the number of contact points and potential current interruptions. The shorter fibers, in contrast, likely provide fewer interconnections, resulting in weaker heat buildup [50].

Under a higher voltage of 45 V (Figure 7 (b)), the difference in thermal output became even more pronounced. The 15 mm fiber specimens achieved a surface temperature of 55.6 °C after 45 minutes, while 10 mm and 5 mm fiber specimens reached only 44.5 °C and 32.9 °C, respectively. These results suggest that the benefits of longer fibers are amplified as the electrical input increases, likely due to greater resistance-induced Joule heating along extended fiber paths. The steeper temperature gradient between fiber lengths under 45 V confirms that fiber geometry is not only influential, but also voltage-sensitive.

At 60 V (Figure 7 (c)), the advantage of longer fibers was again evident, although the gap between fiber lengths narrowed slightly in early-stage heating. After 15 minutes, the 15 mm fibers led to 37.9 °C, closely followed by 10 mm fibers at 36.0 °C, and 5 mm fibers at 31.3 °C. However, by

ARTICLE IN PRESS

the 45-minute mark, the longer fibers again established a clear lead: 57.0 °C for 15 mm, compared to 49.4 °C for 10 mm and 41.1 °C for 5 mm. The convergence in short-term heating performance may be attributed to the rapid conductivity activation at higher voltage levels, which temporarily compensates for the structural limitations of shorter fibers. Yet over time, the cumulative resistive effect in longer fibers dominates, resulting in greater thermal output.

Based on Figure 7(a–c), the temperature rise increases in a slightly super-linear manner with the applied voltage. This behavior suggests that the composite does not maintain a constant effective resistance during heating. As the electrical field becomes stronger, additional fibre–fibre and fibre–matrix contact points become active, which enhances the connectivity of the conductive network and reduces the effective resistivity. Consequently, a larger fraction of the input electrical energy is converted into heat, causing the temperature response to grow faster than what the V^2 relationship alone would predict [51].

Overall, the data indicate that carbon fiber length is a decisive factor in determining heating performance, particularly when the electrical input is elevated and the matrix porosity is held constant. Longer fibers enhance conductive continuity while introducing enough interfacial resistance to maximize localized Joule heating. In contrast, shorter fibers may be too fragmented to sustain strong thermal pathways. The superior thermal response of longer discontinuous fibers can be further understood within the framework of percolation theory. At a fixed volume fraction, fibers with higher aspect ratios (i.e., longer lengths) require fewer individual contacts to form a spanning conductive network across the matrix. This lowers the percolation threshold and enhances the likelihood of establishing continuous pathways through which charge carriers can traverse. The role of contact resistance and percolation is discussed based on established mechanisms reported in the literature and on the consistent thermal trends observed in the present experiments. Percolation is therefore used as a conceptual framework rather than as a quantitatively identified threshold, since no direct electrical characterization was performed. While Joule heating is expected to dominate the thermal response, it is possible that longer fibers also introduce secondary effects such as interfacial polarization or localized charge accumulation under AC excitation. These mechanisms are likely modest compared to resistive heating but may still contribute to the overall temperature rise, particularly at higher voltages where fiber–matrix interfaces become more active. Although quantifying these effects lies beyond the scope of the present work, acknowledging their potential presence provides a more complete interpretation of

ARTICLE IN PRESS

the observed trends. These findings underscore the importance of optimizing fiber geometry—not just content or dispersion—when designing electrically responsive cementitious materials.

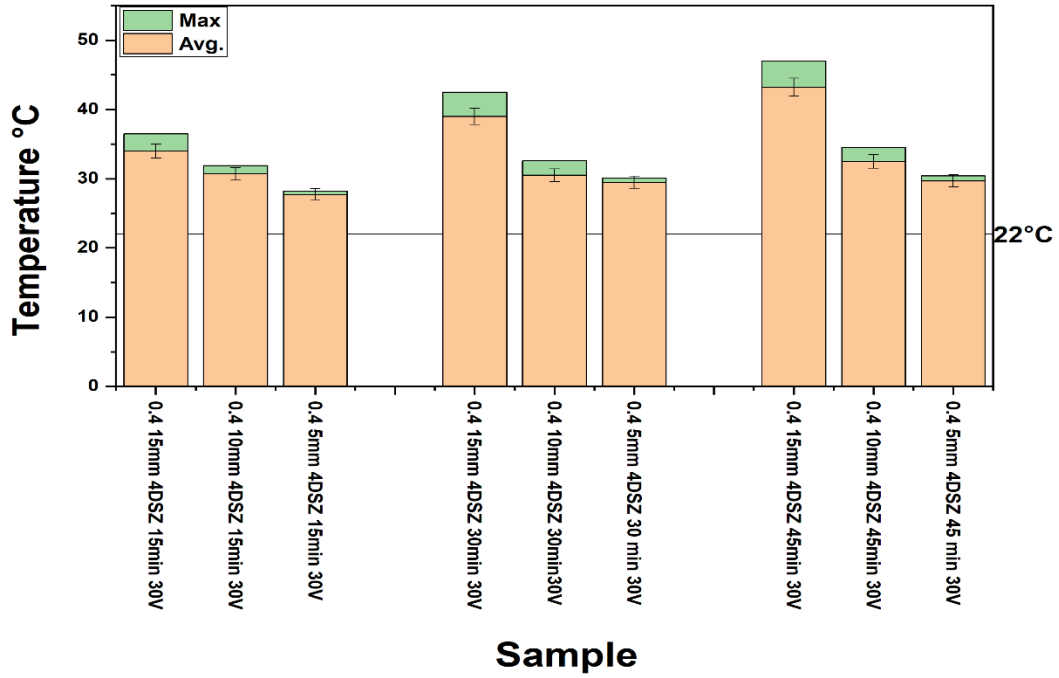

(a)

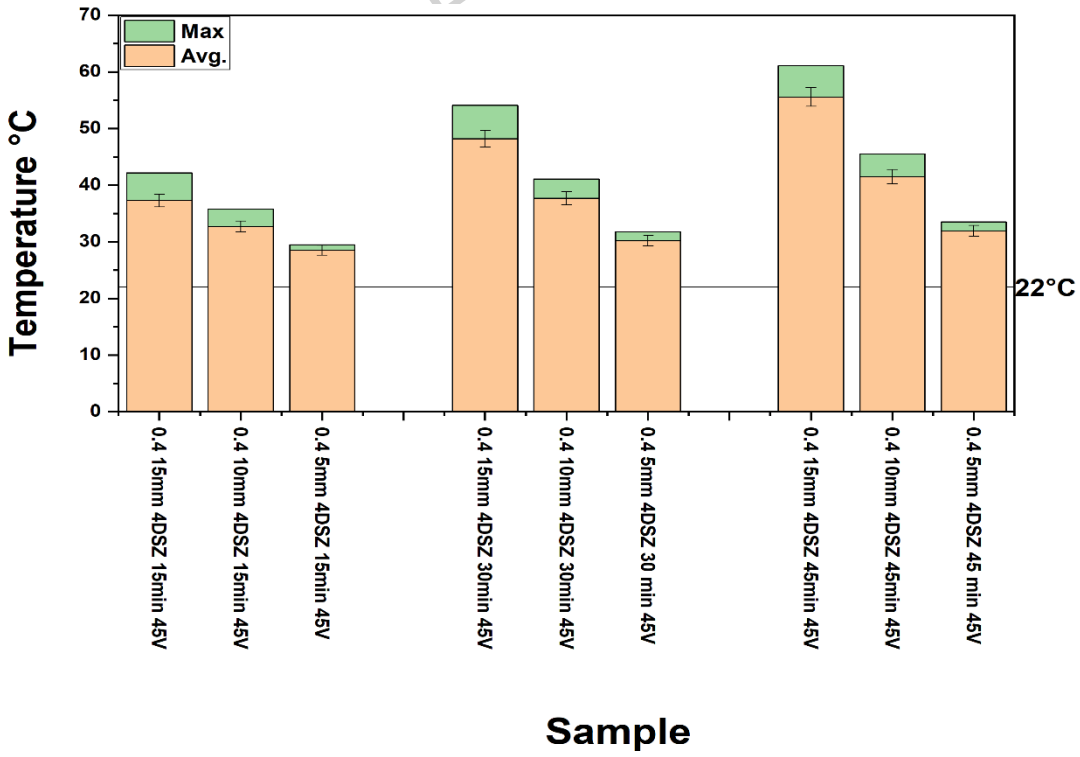

ARTICLE IN PRESS

(b)

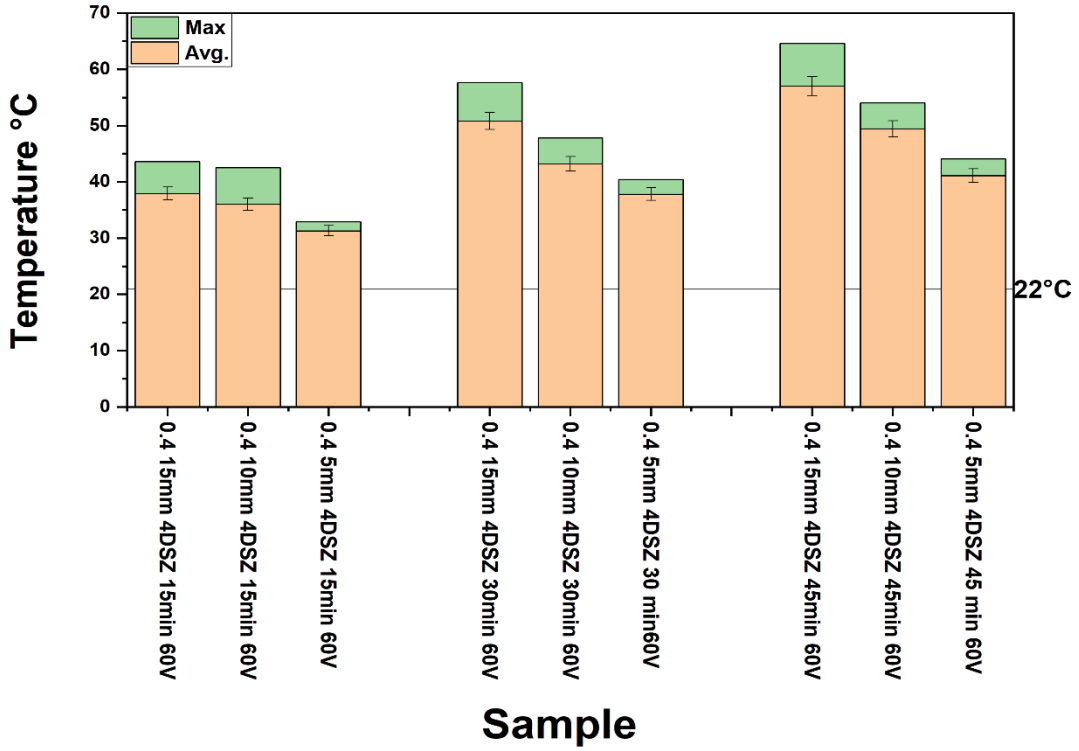

(c)

Figure 7. Heating performance of cement paste specimens reinforced with discontinuous carbon fibers of varying lengths (5 mm, 10 mm, and 15 mm) at a fixed water-to-cement ratio of 0.40: (a) under 30 V, (b) under 45 V, (c) under 60 V.

To enable a clearer comparison among fiber types, fiber lengths, and dosages, the thermal results are evaluated using the normalized metric ΔT/(V·%fiber). The normalized parameter ΔT/(V·%fiber) is used as a comparative indicator rather than a representation of absolute Joule heating efficiency. It does not assume linear scaling of heating with voltage or fiber content, but serves to facilitate relative comparison among specimens tested under identical electrical conditions. This approach separates the intrinsic heating contribution of the fiber network from the influence of applied voltage and fiber volume fraction. The normalized values reveal consistent differences between fiber architectures. For instance, at 30 V and 0.21% fiber content, the discontinuous specimen reaches a normalized value of 1.75, whereas the continuous counterpart yields 1.44. A similar pattern appears across all voltage levels. Increasing the fiber length further

ARTICLE IN PRESS

enhances performance: at 0.28% fiber and 30 V, the normalized values for 15 mm, 10 mm, and 5 mm fibers are 2.52, 1.25, and 0.92 respectively, indicating the stronger resistive network formed by longer fibers. Although ΔT increases with voltage, normalization shows that voltage does not proportionally improve fiber efficiency, confirming that fiber geometry and dispersion dominate the heating response. This metric therefore provides a consistent basis for interpreting the contribution of fiber morphology to the electrothermal behavior of the composites.

4. Conclusion

This study demonstrates that the electrothermal response of carbon-fiber-reinforced cement-based composites is governed primarily by the architecture of the conductive network rather than by electrical conductivity alone. While continuous fibers establish highly aligned, low-resistance pathways that facilitate current transport, this configuration restricts the distribution of Joule heating within the matrix. In contrast, discontinuous fibers create a dense network of fiber–fiber and fiber–matrix contacts, promoting resistive pathways that dissipate electrical energy more uniformly and effectively. The enhanced heating observed with longer fibers and higher dosages further confirms the critical role of contact density and network complexity, whereas increased w/c ratios reduce performance by disrupting conductive continuity through elevated porosity.

These findings clarify the fundamental mechanism underlying self-heating behavior in cementitious composites and provide practical principles for material design. An effective electrothermal system requires a conductive network that is sufficiently interconnected to sustain current flow yet resistive enough to generate meaningful heat. This balance is best achieved using well-dispersed discontinuous fibers of adequate length in a dense matrix with controlled porosity. Such configurations are particularly well suited for winter-resilient pavements, de-icing systems, and building-integrated thermal elements where reliable and efficient resistive heating is required.

Beyond the immediate results, the study highlights several avenues for further research that hold importance for real-world implementation. In the present work, electrical resistivity measurements are not included because the experimental program focuses on comparing the thermal response of different fiber configurations under controlled voltage inputs. Although resistivity data provide a quantitative correlation between electrical conductivity and heating behavior, the consistent trends observed across all mixes still offer meaningful insight into the influence of fiber morphology and matrix porosity. Future studies include direct resistivity testing to more clearly characterize conductive network formation and to strengthen the mechanistic interpretation of Joule heating.

ARTICLE IN PRESS

Long-term cyclic performance, moisture-dependent conductivity evolution, and the environmental durability of fiber networks also require evaluation under realistic service conditions. Further research additionally examines hybrid conductive reinforcements, large-scale casting effects, and system-level integration of these composites into functional electrothermal infrastructures. Advancing these areas supports the development of next-generation multifunctional cementitious materials capable of delivering robust, energy-efficient, and climate-responsive performance.

Data Availability Statement

All data, models, and code generated or used during the study appear in the submitted article.

Competing interests

The authors declare that they have no competing interests.

Acknowledgments

The authors would like to express their sincere thanks to Omnea Abdulhamid Ali Elatrash for her valuable assistance during the experimental studies.

Funding: This study was supported by The Scientific and Technological Research Council of Turkey (TÜBİTAK) under the project number 224M051.

ARTICLE IN PRESS

Reference

1. Makul, N. Introduction to the Principles of Cement and Concrete Composites. in *Principles of Cement and Concrete Composites* (ed. Makul, N.) 1–27 (Springer International Publishing, Cham, 2021). doi:10.1007/978-3-030-69602-3_1.
2. Chen, Y., Tong, J., Li, Q., Xu, S. & Shen, L. Application of High-Performance Cementitious Composites in Steel-Concrete Composite Bridge Deck Systems: A Review. *Journal of Intelligent Construction* **2**, 1–23 (2024).
3. Jin, F., Huang, D., Lino, M. & Zhou, H. A Brief Review of Rock-Filled Concrete Dams and Prospects for Next-Generation Concrete Dam Construction Technology. *Engineering* **32**, 99–105 (2024).

ARTICLE IN PRESS

4. Yang, J., Zhang, Y. & Huang, J. The strengthening theory of steel fiber reinforced concrete and its application in tunnel engineering: A review. *Journal of Engineered Fibers and Fabrics* **19**, 15589250241239242 (2024).
5. Fang, M. *et al.* Discretization and assembly connection technology of cement concrete pavement structure: A review. *Journal of Road Engineering* https://doi.org/10.1016/j.jreng.2024.12.009 (2025) doi:10.1016/j.jreng.2024.12.009.
6. Feng, D. *et al.* Multifunctional performance of carbon nanotubes in thermal energy storage materials. *Materials Today* **75**, 285–308 (2024).
7. Kumar, R. *et al.* Bioinspired and Multifunctional Tribological Materials for Sliding, Erosive, Machining, and Energy-Absorbing Conditions: A Review. *Biomimetics* **9**, 209 (2024).
8. Simões, S. High-Performance Advanced Composites in Multifunctional Material Design: State of the Art, Challenges, and Future Directions. *Materials* **17**, 5997 (2024).
9. Song, F., Li, Q. & Xu, S. A review of self-sensing ultra-high performance concrete: Towards next-generation smart structural materials. *Cement and Concrete Composites* **145**, 105350 (2024).
10. Abden, M. J., Tam, V. W. Y., Afroze, J. D. & Le, K. N. Energy efficient sustainable concrete for multifunctional applications. *Construction and Building Materials* **418**, 135213 (2024).
11. Abedi, M. *et al.* An advanced cement-based geocomposite with autonomous sensing and heating capabilities for enhanced intelligent transportation infrastructure. *Construction and Building Materials* **411**, 134577 (2024).
12. Gao, X. *et al.* Advancing energy solutions: Carbon-based cementitious composites in energy storage and harvesting. *Journal of Building Engineering* **91**, 109720 (2024).
13. Chung, D. D. L. & Ozturk, M. Spatially resolved capacitance-based stress self-sensing in concrete. *ISA Transactions* **152**, 299–307 (2024).

ARTICLE IN PRESS

ARTICLE IN PRESS

14. Ozturk, M. Capacitance-based structural self-sensing of stress: effect of water/cement. *Phys. Scr.* **99**, 075015 (2024).
15. Ozturk, M. A novel method for temperature self-sensing of reinforced concrete. *Phys. Scr.* **99**, 025938 (2024).
16. Ozturk, M. & Chung, D. D. L. Piezopermittivity of cement mortar with various water contents and its application to capacitance-based structural self-sensing of stress. *Sensors and Actuators A: Physical* **369**, 115206 (2024).
17. Ozturk, M. & Xi, X. Exploring the Capacitance-Based Stress Self-Sensing Mechanism in Geopolymer Mortar and Its Correlation with Stress Levels. *J. Electron. Mater.* **53**, 5629–5636 (2024).
18. Ozturk, M. & Xi, X. Enhancing Capacitive Self-sensing Ability of Cement Mortar by Designing Electrode Configuration. *J. Electron. Mater.* https://doi.org/10.1007/s11664-024-11722-5 (2025) doi:10.1007/s11664-024-11722-5.
19. Ozbey, O. D. & Ozturk, M. Exploring capacitance-based stress and deformation sensing in asphalt for smart infrastructure. *Nondestructive Testing and Evaluation* **0**, 1–18.
20. Amran, M. *et al.* Self-Healing Concrete as a Prospective Construction Material: A Review. *Materials* **15**, 3214 (2022).
21. Hossain, Md. R. *et al.* Self-healing concrete for sustainable buildings. A review. *Environ Chem Lett* **20**, 1265–1273 (2022).
22. Nguyen, M.-T. *et al.* Toward Self-Healing Concrete Infrastructure: Review of Experiments and Simulations across Scales. *Chem. Rev.* **123**, 10838–10876 (2023).
23. Afgan, S. & Bing, C. Scientometric review of international research trends on thermal energy storage cement based composites via integration of phase change materials from 1993 to 2020. *Construction and Building Materials* **278**, 122344 (2021).

ARTICLE IN PRESS

ARTICLE IN PRESS

24. Boquera, L., Castro, J. R., Pisello, A. L. & Cabeza, L. F. Research progress and trends on the use of concrete as thermal energy storage material through bibliometric analysis. *Journal of Energy Storage* **38**, 102562 (2021).
25. Rashid, F. L. *et al.* A Review of Recent Improvements, Developments, Effects, and Challenges on Using Phase-Change Materials in Concrete for Thermal Energy Storage and Release. *Journal of Composites Science* **7**, 352 (2023).
26. Wang, S. *et al.* Thermal energy storage in concrete: Review, testing, and simulation of thermal properties at relevant ranges of elevated temperature. *Cement and Concrete Research* **166**, 107096 (2023).
27. Ozturk, M. & Karabulut, A. Electromagnetic Interference Shielding Properties of Carbon Fiber Mortars with Mill Scale and Red Mud: A Comparative Study. *Construction and Building Materials* **451**, 138827 (2024).
28. Öztürk, M. Electromagnetic shielding enhancement in cement composites: a comparative study of mechanically and thermally recycled carbon fibers. *Physica Scripta* **100**, 015047 (2024).
29. Xi, X. *et al.* First study of quantitative relationship between electric polarization and electromagnetic interference (EMI) shielding effectiveness of CFRP. *Carbon* **225**, 119095 (2024).
30. Cao, Z., Dong, W., Öztürk, M., Yang, X. & Xi, X. Sludge-based carbon as an effective admixture in alkali-activated cementitious composites to shield electromagnetic radiation. *Construction and Building Materials* **489**, 142319 (2025).
31. Chung, D. D. L. Self-heating structural materials. *Smart Mater. Struct.* **13**, 562 (2004).
32. Chang, C., Ho, M., Song, G., Mo, Y.-L. & Li, H. A feasibility study of self-heating concrete utilizing carbon nanofiber heating elements. *Smart Mater. Struct.* **18**, 127001 (2009).

ARTICLE IN PRESS

ARTICLE IN PRESS

33. Gwon, S., Moon, J. & Shin, M. Self-heating capacity of electrically conductive cement composites: Effects of curing conditions. *Construction and Building Materials* **353**, 129087 (2022).

34. Xuan, X. Joule heating in electrokinetic flow. *ELECTROPHORESIS* **29**, 33–43 (2008).

35. Chung, D. D. L. Electrically conductive cement-based materials. *Advances in Cement Research* **16**, 167–176 (2004).

36. Pan, P., Wu, S., Xiao, F., Pang, L. & Xiao, Y. Conductive asphalt concrete: A review on structure design, performance, and practical applications. *Journal of Intelligent Material Systems and Structures* **26**, 755–769 (2015).

37. Fulham-Lebrasseur, R., Sorelli, L. & Conciatori, D. Development of electrically conductive concrete and mortars with hybrid conductive inclusions. *Construction and Building Materials* **237**, 117470 (2020).

38. Rahman, M. L., Malakooti, A., Ceylan, H., Kim, S. & Taylor, P. C. A review of electrically conductive concrete heated pavement system technology: From the laboratory to the full-scale implementation. *Construction and Building Materials* **329**, 127139 (2022).

39. Lu, D., Leng, Z., Lu, G., Wang, D. & Huo, Y. A critical review of carbon materials engineered electrically conductive cement concrete and its potential applications. *International Journal of Smart and Nano Materials* **14**, 189–215 (2023).

40. Li, H. *et al.* Surface modification technologies for promoting the widespread use and recycling of carbon fibers in the construction industry. *TIMS* **3**, 100149 (2025).

41. Li, H. *et al.* Effect of electrophoretic deposition of micro-quartz on the microstructural and mechanical properties of carbon fibers and their bond performance toward cement. *J Mater Sci* **57**, 21885–21900 (2022).

ARTICLE IN PRESS

ARTICLE IN PRESS

42. Gao, L. *et al.* Highly conductive polymer composites based on controlled agglomeration of carbon nanotubes. *Carbon* **48**, 2649–2651 (2010).

43. Romanov, V. S., Lomov, S. V., Verpoest, I. & Gorbatikh, L. Stress magnification due to carbon nanotube agglomeration in composites. *Composite Structures* **133**, 246–256 (2015).

44. Wang, H. *et al.* Carbon fibers as additives to engineer agglomeration and propagation of aluminized propellants. *Chemical Engineering Journal* **460**, 141653 (2023).

45. Ding, S. *et al.* Self-heating ultra-high performance concrete with stainless steel wires for active deicing and snow-melting of transportation infrastructures. *Cement and Concrete Composites* **138**, 105005 (2023).

46. Dasari, S. S., Sarmah, A., Mee, R. D., Khalfaoui, A. N. & Green, M. J. Joule Heating of Carbon Fibers and Their Composites in Radio-Frequency Fields. *Advanced Engineering Materials* **25**, 2201631 (2023).

47. Xi, X., Ozturk, M. & Chung, D. D. L. DC electric polarization of cured cement paste being unexpectedly hindered by free water. *Journal of the American Ceramic Society* **105**, 1074–1082 (2022).

48. Allam, H., Duplan, F., Amziane, S. & Burtschell, Y. About the self-sensing behavior of smart concrete and its interaction with the carbon fiber percolation status, sand connectivity status and grain size distribution. *Construction and Building Materials* **324**, 126609 (2022).

49. Allam, H., Duplan, F., Amziane, S. & Burtschell, Y. Assessment of manufacturing process efficiency in the dispersion of carbon fibers in smart concrete by measuring AC impedance. *Cement and Concrete Composites* **127**, 104394 (2022).

50. Choi, Y.-W. *et al.* Enhanced electromagnetic interference shielding in cement composites utilizing carbon fiber clustered networks with dual different lengths. *Carbon* **233**, 119887 (2025).

ARTICLE IN PRESS

ARTICLE IN PRESS

51. Ding, S. *et al.* Developing electrothermal energy storage system for building heating by using stainless steel wires reinforced ultra-high performance concrete. *Composites Part A: Applied Science and Manufacturing* **193**, 108832 (2025).

ARTICLE IN PRESS